



Article

Solvothermal Synthesis of Calcium-Deficient Hydroxyapatite via Hydrolysis of α -Tricalcium Phosphate in Different Aqueous-Organic Media

Rasa Karalkeviciene¹, Eva Raudonyte-Svirbutaviciene^{1,2}, Justina Gaidukevic¹, Aleksej Zarkov¹ 
and Aivaras Kareiva^{1,*} 

¹ Institute of Chemistry, Faculty of Chemistry and Geosciences, Vilnius University, Naugarduko St. 24, LT-03225 Vilnius, Lithuania; rasa.karalkeviciene@nvsp.lt (R.K.); eva.raudonyte-svirbutaviciene@chgf.vu.lt (E.R.-S.); justina.gaidukevic@chgf.vu.lt (J.G.); aleksej.zarkov@chgf.vu.lt (A.Z.)

² Institute of Geology and Geography, Nature Research Centre, Akademijos Str. 2, LT-08412 Vilnius, Lithuania

* Correspondence: aivaras.kareiva@chgf.vu.lt

Abstract: In the present work, the effects of various organic solvents (solvent nature and fraction within the solution) and solvothermal conditions on the formation of calcium-deficient hydroxyapatite (CDHA) via hydrolysis of α -tricalcium phosphate (α -TCP) are investigated. The wet precipitation method is applied for α -TCP synthesis, and the hydrolysis reaction is performed in solutions with different water-to-organic solvent ratios under solvothermal conditions at 120 °C for 3 h and at 200 °C for 5 h. Ethyl alcohol, isopropyl alcohol, and butyl alcohol did not inhibit the hydrolysis of α -TCP, while methyl alcohol and ethylene glycol have a more prominent inhibitory effect on the hydrolysis, hence the formation of single-phased CDHA. From all the solvents analysed, ethylene glycol has the highest impact on the sample morphology. Under certain water to ethylene glycol ratios and solvothermal conditions, samples containing a significant fraction of rods are obtained. However, samples prepared with ethylene glycol are characterised by a particularly low BET surface area.

Keywords: calcium hydroxyapatite; α -tricalcium phosphate; water-organic solvent system; solvothermal synthesis



Citation: Karalkeviciene, R.; Raudonyte-Svirbutaviciene, E.; Gaidukevic, J.; Zarkov, A.; Kareiva, A. Solvothermal Synthesis of Calcium-Deficient Hydroxyapatite via Hydrolysis of α -Tricalcium Phosphate in Different Aqueous-Organic Media. *Crystals* **2022**, *12*, 253. <https://doi.org/10.3390/cryst12020253>

Academic Editor:
Carlos Rodriguez-Navarro

Received: 31 January 2022

Accepted: 11 February 2022

Published: 13 February 2022

Publisher's Note: MDPI stays neutral with regard to jurisdictional claims in published maps and institutional affiliations.



Copyright: © 2022 by the authors. Licensee MDPI, Basel, Switzerland. This article is an open access article distributed under the terms and conditions of the Creative Commons Attribution (CC BY) license (<https://creativecommons.org/licenses/by/4.0/>).

1. Introduction

Hydroxyapatite ($\text{Ca}_{10}(\text{PO}_4)_6(\text{OH})_2$, HAp) is a major inorganic component in human hard tissue and is one of the most investigated calcium phosphates (CaPs) [1–3]. Due to its bone-like chemical composition and crystalline structure, HAp is extensively applied as bioceramic material for bone grafting [4,5]. In addition to that, HAp has found applications in drug delivery [6], chromatography [7], and is a very promising material for the treatment of air, water, and soil pollution [8–11]. Since HAp is considered to be an environmentally benign functional material, and due to its remarkable adsorption capacity, HAp could be extremely useful in the field of environmental management [8]. Calcium-deficient hydroxyapatite (CDHA, $\text{Ca}_{10-x}(\text{HPO}_4)_x(\text{PO}_4)_{6-x}(\text{OH})_{2-x}$) is HAp with a Ca/P ratio from 1.50–1.67 [12]. Previous studies have reported a larger specific surface area and superior incorporating efficacy of CDHA when compared to other CaPs [13,14]. The chemical composition of HAp can be modified from the stoichiometric form to the Ca-deficient form by selecting an appropriate Ca/P molar ratio [15].

Solubility, specific surface area, surface wettability, and hence the adsorption characteristics of HAp crystals, depend greatly on their morphology and crystallinity [5,11]. Moreover, HAp contains the following two types of crystal planes: a (b)-plane, rich in positively charged Ca^{2+} ions, and a c-plane, exposing negatively charged phosphate and hydroxyl groups [10]. Hence, if the crystal growth along a specific direction is induced, HAp

could gain new desirable properties and be applied, for instance, as a selective adsorbent of negatively or positively charged compounds [9].

HAp could be obtained via different synthesis methods, including solid-state reactions, sol-gel technology, chemical precipitation, hydrolysis, hydrothermal, or solvothermal methods [2,16–18]. Among them, solvothermal synthesis is probably the most popular method, providing the possibility to obtain well-crystallized, single-phase HAp [1,19,20]. In addition to that, many groups have already reported the solvothermal synthesis of specifically shaped (plate-like and rod-like) HAp crystals using various additives in the reaction solution [1,20–22]. Several groups suggested that various alcohols could be successfully applied as HAp morphology-controlling agents during the solvothermal process. For instance, Goto et al. [16] has reported the synthesis of needle-like HAp crystals using ethyl alcohol-water solutions. Guo et al. [23] has observed that isopropyl alcohol has affected the crystallite size and crystallinity degree of the HAp crystals but had little effect on the sample morphology. However, as far as we know, no comprehensive study has ever been performed to compare the effects of different organic solvents on the hydrolysis of α -tricalcium phosphate (α -TCP) under solvothermal conditions. In this study, we aim to fill in this gap. To this end, solvothermal reactions were performed with different proportions of water-organic solvent. The organic solvents used were as follows: ethylene glycol, methyl alcohol, ethyl alcohol, isopropyl alcohol, and butyl alcohol. The effects of the solvothermal conditions, nature of the solvent, and organic solvent fraction in the solution on the phase purity and morphological features of HA were investigated.

2. Materials and Methods

2.1. Synthesis

First, metastable α -TCP was synthesized by wet precipitation method as a precursor for the further conversion to CDHA. An appropriate amount (3.42 g) of calcium nitrate tetrahydrate ($\text{Ca}(\text{NO}_3)_2 \cdot 4\text{H}_2\text{O}$, $\geq 99\%$, Roth, Karlsruhe, Germany) was dissolved in 20 ml of deionized water. A portion (1.27 g) of diammonium hydrogen phosphate ($(\text{NH}_4)_2\text{HPO}_4$, $\geq 98\%$, Roth, Karlsruhe, Germany) was dissolved in 15 ml of deionized water in a separate beaker. After dissolution, concentrated ammonium hydroxide (NH_4OH , 25%, Roth, Karlsruhe, Germany) was added to the latter solution until pH of the solution reached 10. After stirring for one minute, an aqueous solution of $\text{Ca}(\text{NO}_3)_2 \cdot 4\text{H}_2\text{O}$ was added rapidly. A white precipitate formed, which was stirred for 10 minutes at 400 rpm. The obtained precipitate was subsequently vacuum filtered and washed with an appropriate volume of deionized water and isopropyl alcohol [24]. The synthesis product was dried overnight in an oven at 50 °C. The dried powders were ground in agate mortar and annealed in a furnace at 700 °C for 5 h at a heating rate of 5 °C/min.

Solvothermal reactions were performed with different proportions of water and ethylene glycol (EG, $>99\%$, Roth, Karlsruhe, Germany), water-methyl alcohol (MeOH, $>99.9\%$, Roth, Karlsruhe, Germany), water-ethyl alcohol (EtOH, $>96\%$, Roth, Karlsruhe, Germany), water-isopropyl alcohol (PrOH, $>99.5\%$, Roth, Karlsruhe, Germany), and water-butyl alcohol (BuOH, $>99.5\%$, Roth, Karlsruhe, Germany). The water to alcohol *v/v* ratios of 0:100, 20:80, 40:60, 60:40, and 80:20 were applied. For the synthesis, 0.3 g of α -TCP powder was placed into 90 ml polytetrafluoroethylene-lined stainless-steel pressure vessels and diluted with 20 ml of water-organic solvent mixture. Solvothermal treatment was performed at 120 °C for 3 h and at 200 °C for 5 h. Finally, the resulting powders were filtered, washed with EtOH, and dried at 50 °C overnight.

The sample notations and treatment conditions are given in Table 1. Water to alcohol *v/v* ratios of 0:100, 20:80, 40:60, 60:40, and 80:20; 100:0 were applied to all the solvents under both conditions of solvothermal treatment.

Table 1. Sample codes, solvents applied, and solvothermal treatment conditions.

Notation	Solvothermal Conditions	Organic Solvent Applied	Water-to-Organic Solvent (W:O)
120-W-EG	120 °C, 3 h	ethylene glycol	
120-W-MeOH	120 °C, 3 h	methyl alcohol	
120-W-EtOH	120 °C, 3 h	ethyl alcohol	0:100
120-W-PrOH	120 °C, 3 h	isopropyl alcohol	20:80
120-W-BuOH	120 °C, 3 h	butyl alcohol	40:60
200-W-EG	200 °C, 5 h	ethylene glycol	60:40
200-W-MeOH	200 °C, 5 h	methyl alcohol	80:20
200-W-EtOH	200 °C, 5 h	ethyl alcohol	0:100
200-W-PrOH	200 °C, 5 h	isopropyl alcohol	
200-W-BuOH	200 °C, 5 h	butyl alcohol	

2.2. Characterization

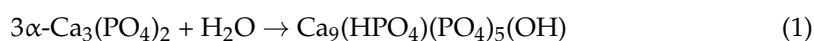
Powder X-ray diffraction data were collected on a Rigaku MiniFlex II diffractometer (Rigaku, The Woodlands, TX, USA) operating in Bragg–Brentano ($\theta/2\theta$) geometry, using Ni-filtered Cu $K\alpha$ radiation. The data were collected within a 2θ angle range from 10 to 60° at a step width of 0.01° and speed of 5°/min. Infrared (FTIR) spectra were recorded in the range of 4000–400 cm^{-1} employing Bruker ALPHA ATR spectrometer (Bruker, Billerica, Ma, USA). In order to study the morphology of the samples, a field-emission scanning electron microscope (FE-SEM) Hitachi SU-70 (FE-SEM, Hitachi, Tokyo, Japan) was used.

Textural properties of the prepared samples were estimated from N_2 adsorption/desorption isotherms at -196 °C using a Micromeritics TriStar 3020 analyser (Micromeritics, Norcross, GA, USA). Before the measurements, all the samples were outgassed in the N_2 atmosphere at 100 °C. The total surface area (S_{BET}) was estimated using the Brunauer–Emmet–Teller (BET) equation, while Barrett–Joyner–Halenda (BJH) equation was used to calculate pore size distribution of the samples [25].

3. Results and Discussion

The characteristics of the α -TCP precursor are presented in Figure 1. As it could be seen from the XRD diffraction pattern (Figure 1a), all the peaks match the standard XRD data of monoclinic $\text{Ca}_3(\text{PO}_4)_2$ (ICDD #00-070-0364) very well. The starting powders consisted of agglomerates of nanodimensional, mostly uniform elongated particles of irregular shape (Figure 1c). The sample exhibited type IV isotherms and displayed an H3 hysteresis loop (Figure 1b). Based on the pore size distribution results, illustrated in the inset image of Figure 1b, the sample was mainly characterised by pores smaller than 10 nm, albeit larger pores up to 55 nm were also present. The BET surface area (S_{BET}) of the precursor was 10.22 $\text{m}^2 \text{g}^{-1}$.

Under the reaction with water, α -TCP hydrolyses and converts to CDHA as described by the following equation [16]:



A sufficient amount of water is required for the first stage to occur. The phase crystallinity and purity of synthesized CDHA powders were investigated by XRD analysis, which revealed some differences among the obtained products. The samples treated with organic solvent only (0:100) showed no evidence of CDHA formation. Due to the absence of water, no hydrolysis reaction occurred, and the phase of such samples remained α -TCP (ICDD 00-070-0364). This was true for all the organic solvents used under different solvothermal treatments.

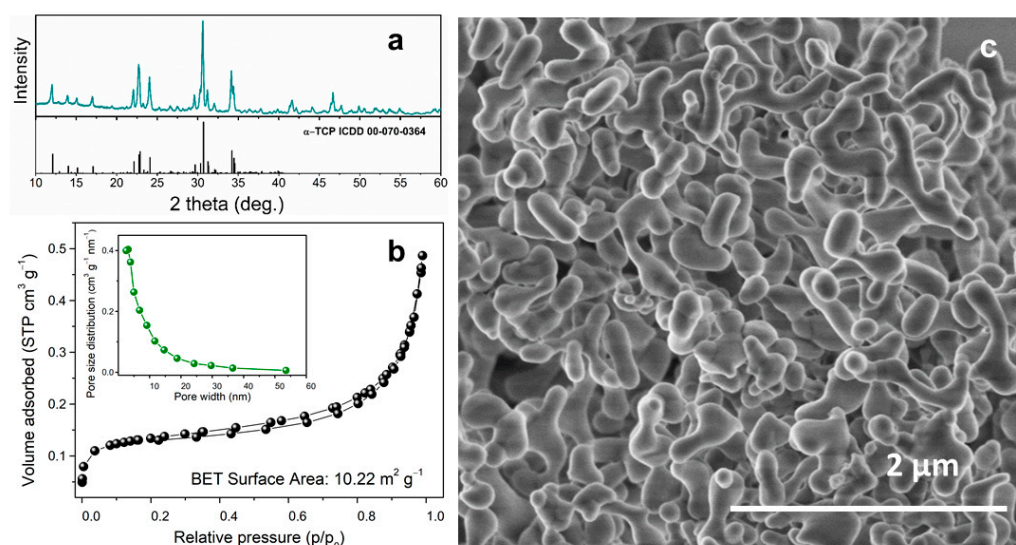


Figure 1. Characteristics of the obtained α -TCP precursor: XRD pattern (a), nitrogen adsorption-desorption isotherms and the corresponding BJH pore-size distribution (b), and SEM image (c).

In the case of EtOH, PrOH, and BuOH, the introduction of even a small fraction (20:80) of water resulted in the formation of single-phased CDHA (ICDD 00-76-0694), while an increasing water content provided the same results. This was observed under various applied solvothermal conditions. Under harsher solvothermal conditions (200 °C for 5 h), the formation of monetite was observed in the presence of EtOH, PrOH, and BuOH. This was especially notable in the case of BuOH. For comparison between the solvents, XRD patterns of the samples prepared under different solvothermal conditions using a W:O ratio of 40:60 are given in Figure 2 as representative.

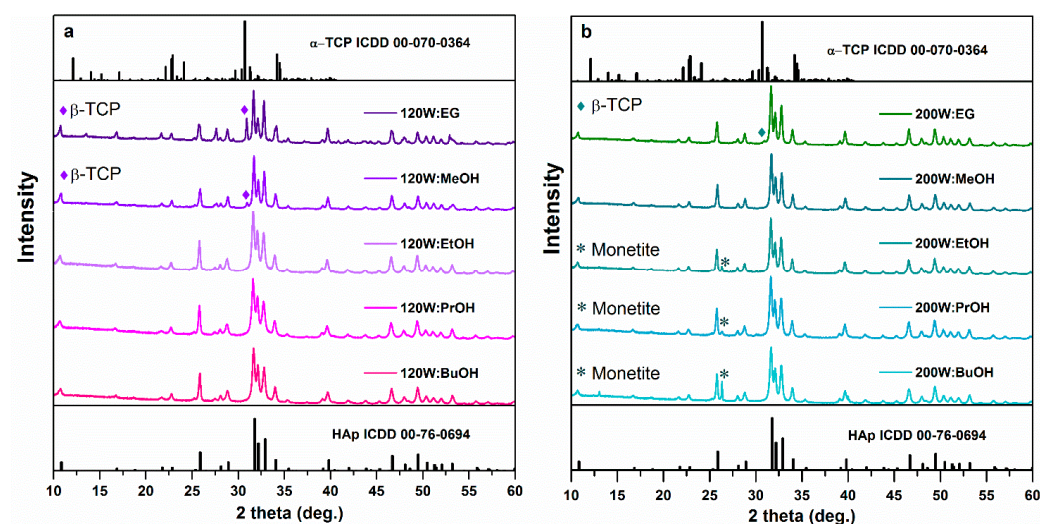


Figure 2. XRD patterns of the samples prepared using water-to-organic solvent ratio of 40:60 after a solvothermal treatment at 120 °C for 3 h (a) and at 200 °C for 5 h (b).

In contrast, MeOH and EG had a stronger inhibitory effect on α -TCP hydrolysis. These effects were especially notable for EG under the milder solvothermal conditions. Figure 3 shows the powder XRD patterns of the samples prepared under different solvothermal treatments (120 °C for 3 h and 200 °C for 5 h) using varying water to MeOH and water to EG ratios. After a treatment at 120 °C for 3 h, the sample with a water to EG ratio of 20:80 remained a single phase α -TCP (ICDD 00-070-0364, Figure 3b). Increasing water content induced the formation of CDHA, but a strong peak attributed to β -tricalcium

phosphate (β -TCP, ICDD 00-070-2065) was visible in the sample 120-W-EG-40:60, while only a trace of β -TCP could be observed in the XRD pattern of 120-W-EG-60:40 (Figure 3b). MeOH has also inhibited the formation of CDHA, albeit to a lesser extent. The sample 120-W-MeOH-20:80 contained large fractions of CDHA, β -TCP and α -TCP. Traces of β -TCP were detected in the sample 120-W-MeOH-40:60, while the samples with a larger amount of water consisted of single-phase CDHA (Figure 3a).

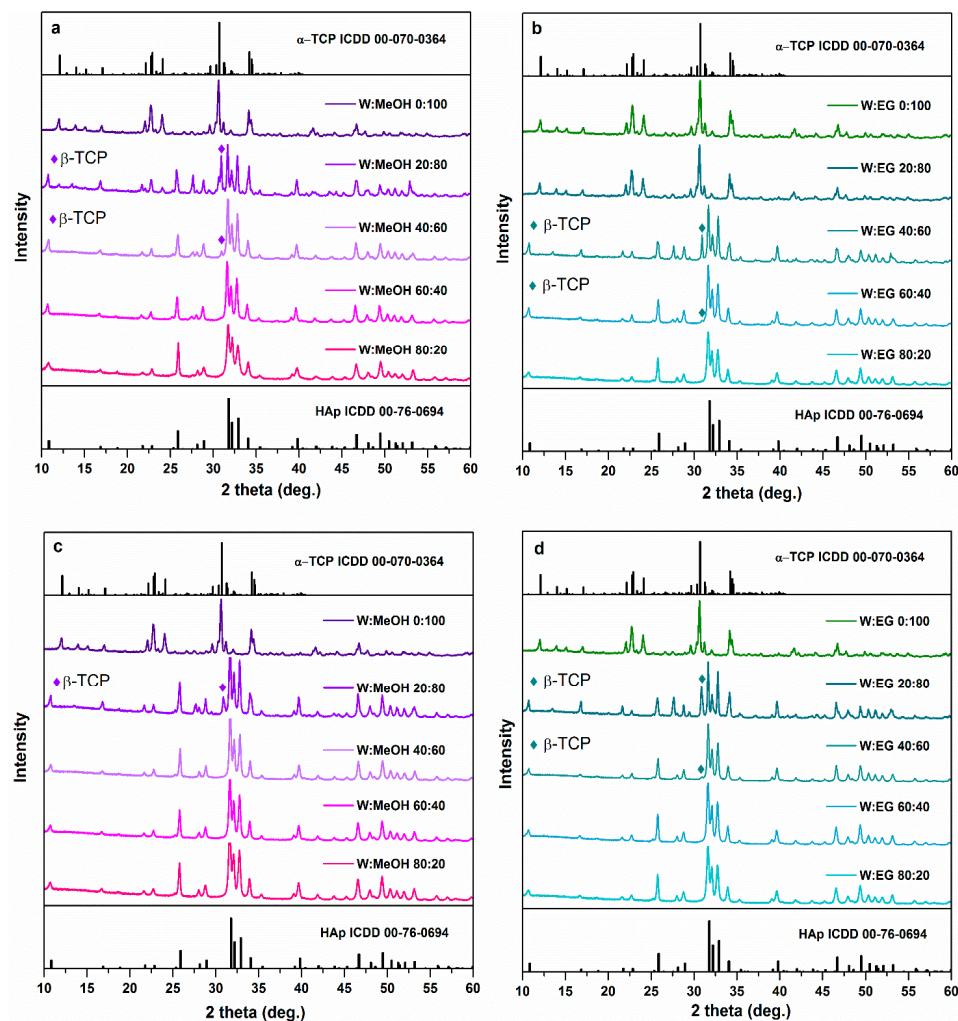


Figure 3. XRD patterns of the samples prepared using different water to MeOH (a,c) and water to EG (b,d) ratios under the following different solvothermal conditions: 120 °C for 3 h (a,b) and 200 °C for 5 h (c,d).

The increased temperature and prolonged time of the solvothermal synthesis caused the following shift in the inhibitory effect: single-phase CDHA was observed for the sample 200-W-EG-60:40, only a trace of β -TCP was detected in the XRD pattern of 200-W-EG-40:60, whereas the formation of CDHA was also obvious in 200-W-EG-20:80, even though a significant fraction of β -TCP was still present in the latter sample (Figure 3d). A higher temperature and longer reaction time have also resulted in a decreased β -TCP fraction in the sample 200-W-MeOH-20:80 (Figure 3c).

The FTIR spectra of the products prepared by the solvothermal treatment are presented in Figure 4. The FTIR range of 1500–400 cm^{-1} was chosen as representative since the main bands attributed to HAp and TCP polymorphs could be observed in this region, and the differences between the samples were hardly distinguishable in the full range spectra. The stretching modes of the hydroxyl group usually observed at 3572 cm^{-1}

were hardly visible in our case, and their intensity was similar in all the samples [26]. Several absorption bands at around 1095–960 and 636–550 cm^{-1} were observed in all the samples. The bands centred at 561–556 and 603–599 cm^{-1} are assigned to ν_4 O–P–O bending mode of CDHA [3]. Bands centred at 1020–1017 and 1090–1084 cm^{-1} correspond to ν_3 asymmetric P–O stretching vibrations, while the peak centred at 961–960 cm^{-1} corresponds to symmetric P–O stretching vibrations (ν_1) of CDHA [3]. The peak centred at 633–625 cm^{-1} corresponds to the bending vibrational mode of the hydroxyl (–OH) group [3,16]. An absorption band centred at 871–868 cm^{-1} is assigned to the P–O(H) stretching mode of the HPO_4^{2-} group, which is present in the structure of calcium-deficient CDHA [12]. The aforementioned bands were visible in the FTIR spectra of all the samples.

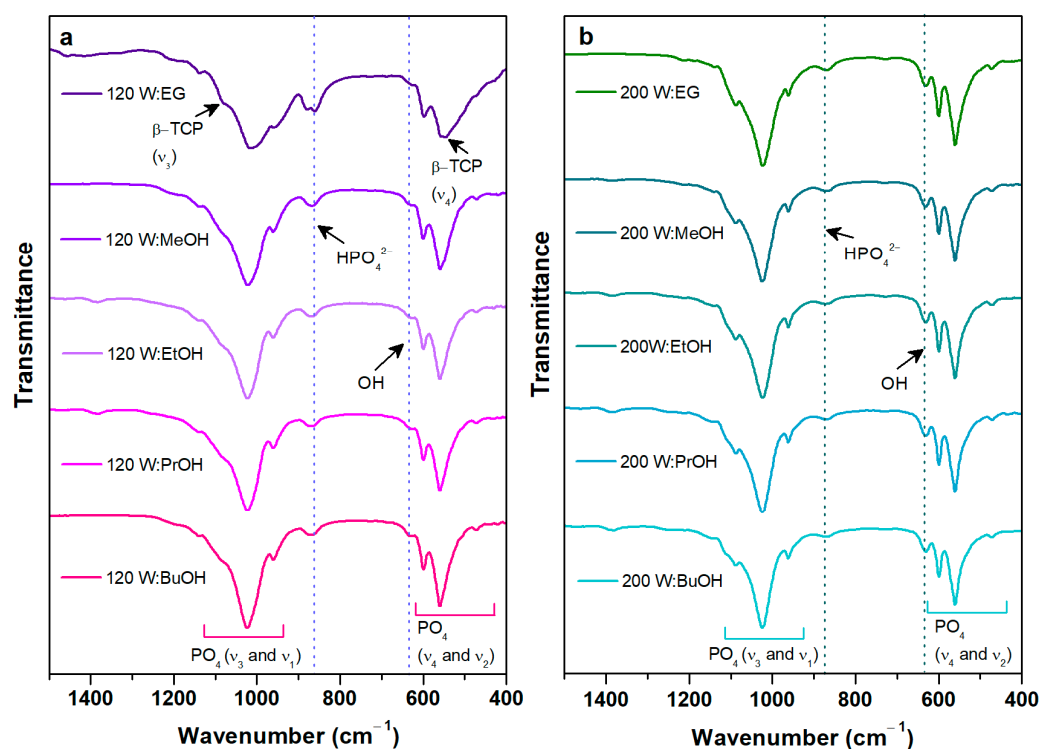


Figure 4. FTIR spectra of the samples prepared using water-to-organic solvent ratio of 40:60 after solvothermal treatment at 120 °C for 3 h (a) and at 200 °C for 5 h (b).

The additional bands attributed to β -TCP phase were only visible in the FTIR spectra of the samples prepared using larger fractions of EG (120-W-EG-20:80; 120-W-EG-40:60; 200-W-EG-20:80). As it could be seen from Figure 4a, bands at 544 and 1083 cm^{-1} of the sample 120-W-EG-40:60 could be attributed to β -TCP phase (ν_4 and ν_3 , respectively) [27]. Such results are in agreement with the XRD data.

The morphology of the obtained samples varied from plate-shaped to rod-shaped. Samples fabricated without organic solvents consisted of plate-shaped crystals arranged into flower-like structures. In this study, only slight effects on morphology were observed due to the introduction of EtOH and PrOH. Under the milder solvothermal conditions (120 °C for 3 h), large proportion of EtOH and PrOH (120-W-EtOH-20:80; 120-W-PrOH-20:80) caused the formation of large plates with no prominent self-assembly (Figures S2 and S3). With an increasing proportion of water (W:O 40:60; 60:40; and 80:20), the formation of narrower plates and some rods was observed; moreover, the crystals were arranged in flower-like structures. When the reaction time and temperature were increased, higher proportions of EtOH, PrOH, and BuOH resulted in the formation of rods. Moreover, more rods have formed at the same W:O ratio under harsher conditions. However, plate-like crystals were still prevalent in all of the samples. SEM images of the samples prepared under different solvothermal conditions using a W:O ratio of 40:60 are presented in Figure 5.

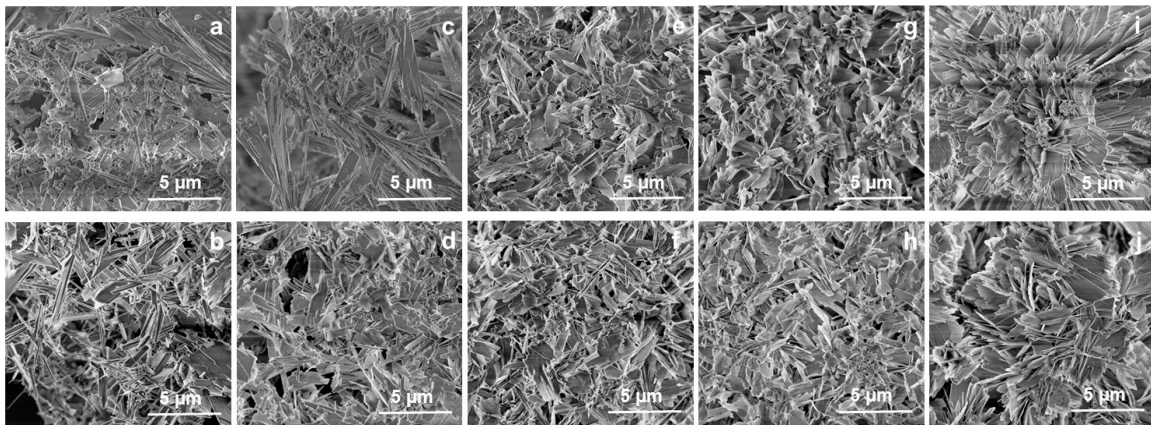


Figure 5. SEM images of the samples after solvothermal treatment with W:O ratio 40:60: (a) 120-W-EG-40:60; (b) 200-W-EG-40:60; (c) 120-W-MeOH-40:60; (d) 200-W-MeOH-40:60; (e) 120-W-EtOH-40:60; (f) 200-W-EtOH-40:60; (g) 120-W-PrOH-40:60; (h) 200-W-PrOH-40:60; (i) 120-W-BuOH-40:60; (j) 200-W-BuOH-40:60.

The use of MeOH (Figures 5c,d and S1) and BuOH (Figure 5i,j) had a more prominent effect on the sample morphology than the previously described solvents (Figures S3 and S4). In this case, the samples were also dominated by plate-like crystals, but a trend of long and narrow plate formation was observed. Moreover, more rods were present in the MeOH and BuOH treated samples when compared to the samples prepared in W-EtOH and W-PrOH solutions.

From all the solvents analysed, EG had the highest impact on the sample morphology. Under the milder solvothermal conditions (120 °C for 3 h), the formation of HAp was completely suspended in the sample 120-W-EG-20:80 (Figure 6c). Sample 120-W-EG-40:60 consisted of large plates, some rods, and some particles of different shapes, which could probably be attributed to β -TCP phase (Figure 6e). Sample 120-W-EG-60:40 was characterised by a large number of rods in addition to the plates (Figure 6g). In contrast, no rods were observed in a sample prepared with a minimal amount of EG (120-W-EG-80:20; Figure 6i). Prolonged reaction time and increased temperature resulted in a rod-dominated morphology of the CDHA samples. The sample 200-W-EG-20:80 was characterised by larger and smaller rods, as well as some minor particles of different shapes, which should be attributed to β -TCP phase (Figure 6d). A slightly lower proportion of EG (samples 200-W-EG-40:60 and 200-W-EG-60:40; Figure 6f,h) resulted in the formation of both plate-shaped and a large number of rod-shaped crystals. No rods were observed in a sample prepared with a minimal amount of EG (200-W-EG-80:20; Figure 6j).

It is assumed that the solvothermally assisted formation of rod-like crystals comprises the following two main stages: the nucleation step (reaction of ions), when small crystalline nuclei are formed in a supersaturated matrix, and the growth step, during which nuclei grow into their final shape and size [28]. In our case, the changes in crystal morphology might be related to the decreased supply of water when more organic solvents are introduced to the system. This would limit the hydrolysis reaction of α -TCP [16]. Previous studies stated that the increasing amount of alcohol in the aqueous reaction solution reduces the solubility of α -TCP and hence limits the supply of Ca^{2+} and PO_4^{3-} ions [16,29,30]. Such an effect is related to the changes in dielectric constant ($\epsilon_r(\omega)$) of the solution: with a decreasing dielectric constant of the solvent, solubility decreases due to the decreased solvation energy [31,32]. Dielectric constant of pure water is 78.5 at 25 °C, whereas the dielectric constants of alcohols are significantly lower. The dielectric constants at 25 °C of the organic solvents used in this study are as follows: $\epsilon_r(\omega)_{\text{EG}} = 38.5$; $\epsilon_r(\omega)_{\text{MeOH}} = 32.70$; $\epsilon_r(\omega)_{\text{EtOH}} = 24.3$; $\epsilon_r(\omega)_{\text{PrOH}} = 19.92$; $\epsilon_r(\omega)_{\text{BuOH}} = 17.5$ [32]. Variations in $\epsilon_r(\omega)$ of water-organic solvent mixtures depend on the composition of the solution, but in general, $\epsilon_r(\omega)$ values decrease with the increasing fraction of organic solvent [33]. Solvents with different

physicochemical properties influence solubility, crystal nucleation, and growth rate, which in turn has an effect on the crystallinity and morphology of the final products [32]. When the hydrolysis reaction is not suspended and the solution is supersaturated with Ca^{2+} and PO_4^{3-} ions, nucleation takes dominance over the crystal growth and smaller crystals are formed. On the contrary, when the supply of Ca^{2+} and PO_4^{3-} ions is limited, fewer nuclei form and larger crystals tend to grow [28,32]. Other properties of different solvents might have also affected the processes of α -TCP hydrolysis and HAp crystallisation. For instance, the presence of EG in the reaction mixture would significantly change the viscosity of the suspension [34,35]. Subsequently, ion mobility and diffusion rates would be reduced, which would in turn inhibit the hydrolysis reaction and retard the nucleation process [35]. The viscosity of the reaction media decreases with the increasing temperature, and thus the inhibitory effects of EG are less significant when the solvothermal synthesis is performed at higher temperatures (Figure 3b,d).

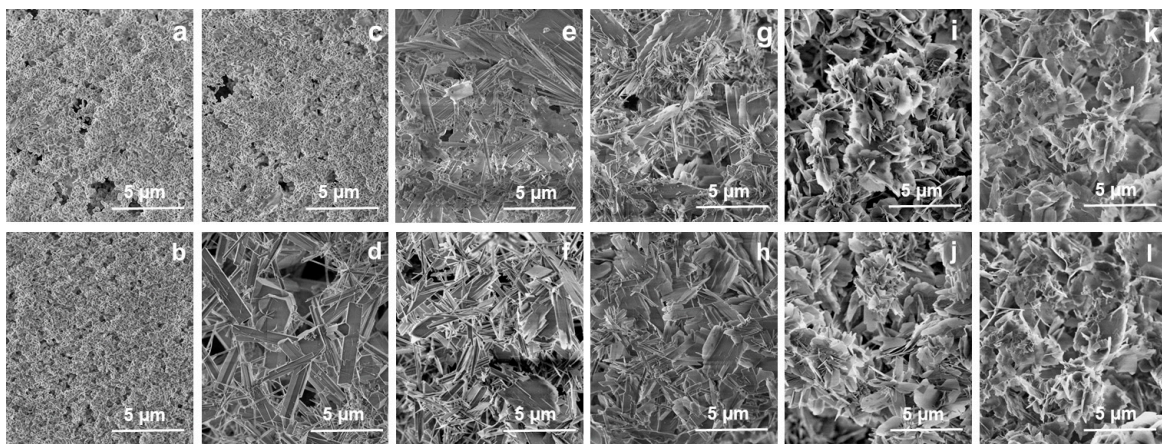


Figure 6. SEM images of the samples prepared with different ratios of water and ethylene glycol: (a) 120-W-EG-0:100; (b) 200-W-EG-0:100; (c) 120-W-EG-20:80; (d) 200-W-EG-20:80; (e) 120-W-EG-40:60; (f) 200-W-EG-40:60; (g) 120-W-EG-60:40; (h) 200-W-EG-60:40; (i) 120-W-EG-80:20; (j) 200-W-EG-80:20; (k) 120-W-EG-100:0; (l) 200-W-EG-100:0.

It is worth noting that the results obtained in this study differ from those reported by Goto et al. [16], who managed to prepare needle-like CDHA crystals arranged into flower-like structures by using water-ethyl alcohol solutions. We assume such discrepancies could originate due to the different starting materials used and slightly different solvothermal conditions applied. In their study, Goto et al. applied commercial α -TCP (Taihei Chemical Industrial Co., Ltd., Osaka, Japan) synthesized at a high temperature and consisting of large particles, while in our study we used low-temperature synthesized metastable α -TCP.

Figure 7 shows the nitrogen adsorption-desorption isotherms and the corresponding BJH pore-size distribution for CDHA particles. According to the new classification by the IUPAC, all the samples exhibited type IV isotherms and displayed H3 hysteresis loops. This type of isotherm indicates the existence of mesopores in the structure of all the samples. The hysteresis loop type H3 is associated with the existence of aggregated plate-like particles [36]. Such results are in agreement with SEM data (Figures 5 and 6). Based on the pore size distribution results illustrated in the inset image of Figure 7a,b, there were no significant differences between the samples. All the samples were characterised by a wide pore size distribution. Multi-scale pores ranged from 2.6 to 128 nm, suggesting that both mesopores and macropores were present in the CDHA structure. All the samples except those prepared with EG contained both mesopores of smaller sizes (from 2.6 nm up to 9.0 nm) and a small number of larger mesopores (from 9.0 nm up to 128 nm). On the contrary, in the sample 120-W-EG-40:60, mainly mesopores of larger width (from 23.0 nm up to 50.2 nm) were found. We assume the pores of smaller sizes presented in the structure of this sample were probably partially blocked by the viscous ethylene glycol. As it can be

seen from Figure 7c, the mesoporous 120-W-PrOH-40:60 had the highest BET surface area (S_{BET}) of $24.3 \text{ m}^2 \text{ g}^{-1}$. An extremely low surface area was observed for the samples prepared using EG: S_{BET} of $2.1 \text{ m}^2 \text{ g}^{-1}$ and $11.3 \text{ m}^2 \text{ g}^{-1}$ were obtained for the samples 120-W-EG-40:60 and 200-W-EG-40:60, respectively. One reasonable explanation for this decrease is that residues of EG may have increased blockage of the nitrogen gas penetration. Moreover, this decrease in S_{BET} could be the result of the structural changes occurring during the synthesis of CDHA. The remaining samples were characterised by similar S_{BET} values ranging from 9.9 to $22.4 \text{ m}^2 \text{ g}^{-1}$.

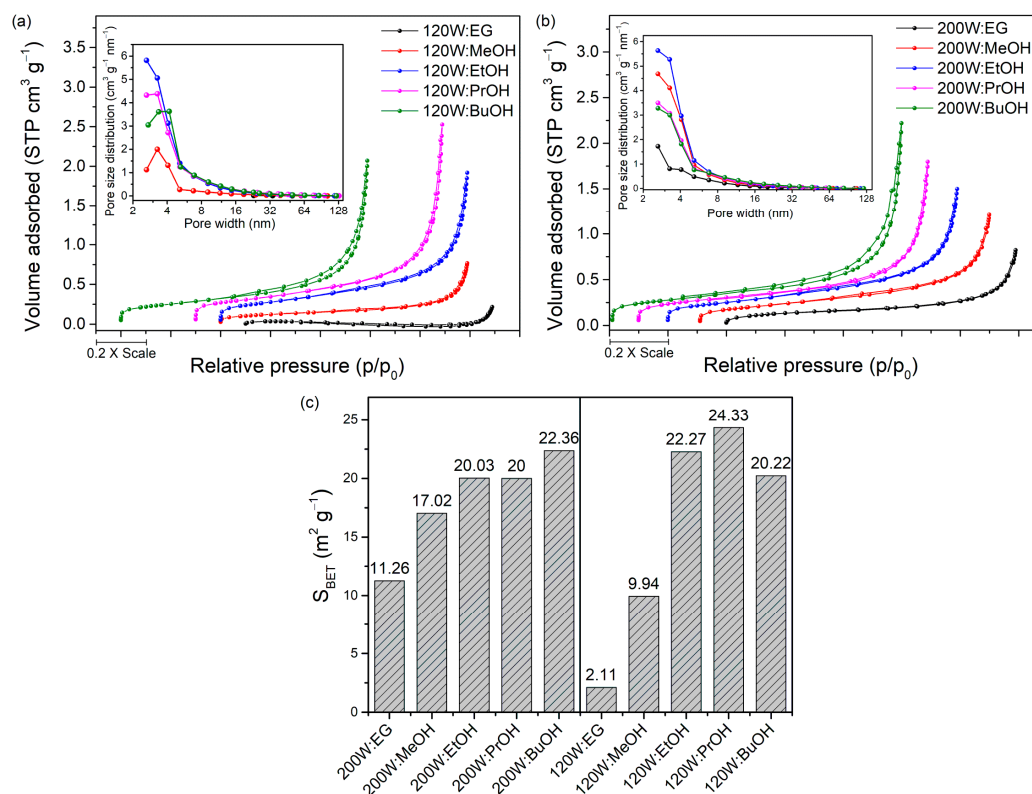


Figure 7. Nitrogen adsorption-desorption isotherms and the corresponding BJH pore-size distribution for the samples after solvothermal treatment with a W:O ratio of 40:60: (a) 120 °C; (b) 200 °C; and (c) BET surface area for the samples after solvothermal treatment with a W:O ratio of 40:60 at 120 °C and 200 °C.

4. Conclusions

A comprehensive study was performed to compare the effects of different organic solvents on the hydrolysis of α -TCP and its conversion to CDHA under different solvothermal conditions. Methyl alcohol and ethylene glycol had a stronger inhibitory effect on α -TCP hydrolysis than ethyl alcohol, isopropyl alcohol, and butyl alcohol. This was especially notable under milder solvothermal conditions. The morphology of the obtained samples varied from plate-shaped to rod-shaped. Samples containing some rods were obtained by applying certain ethyl alcohol and isopropyl alcohol proportions, albeit plate-like structures were still prevailing. The use of water-methyl alcohol and water-butyl alcohol mixtures leads to the formation of more rods in addition to the long and narrow plates. From all the solvents analysed, ethylene glycol had the highest impact on the sample morphology. Under certain water to ethylene glycol ratios and solvothermal conditions, samples containing a significant fraction of rods were obtained.

Supplementary Materials: The following supporting information can be downloaded at: <https://www.mdpi.com/article/10.3390/cryst12020253/s1>, Figure S1: images of the samples after solvothermal treatment with W-MeOH; Figure S2: SEM images of the samples after solvothermal treatment with W-EtOH; Figure S3: SEM images of the samples after solvothermal treatment with W-PrOH; Figure S4: SEM images of the samples after solvothermal treatment with W-BuOH.

Author Contributions: Conceptualization, R.K., E.R.-S., J.G., A.Z. and A.K.; methodology, R.K., E.R.-S. and A.Z., formal analysis, R.K.; investigation, R.K. and J.G., resources, E.R.-S., A.Z. and A.K., data curation, R.K., E.R.-S., J.G., A.Z. and A.K., writing—original draft preparation, E.R.-S., writing—review and editing, R.K., E.R.-S., J.G., A.Z. and A.K., supervision, A.Z. and A.K.; funding acquisition, E.R.-S., A.Z. and A.K. All authors have read and agreed to the published version of the manuscript.

Funding: This research has received funding by the European Social Fund under the No 09.3.3-LMT-K-712 “Development of Competences of Scientists, other Researchers and Students through Practical Research Activities” measure (project No 09.3.3-LMT-K-712-23-0070).

Data Availability Statement: Data is contained within the article.

Conflicts of Interest: The authors declare no conflict of interest.

References

1. In, Y.; Amornkitbamrung, U.; Hong, M.H.; Shin, H. On the Crystallization of Hydroxyapatite under Hydrothermal Conditions: Role of Sebacic Acid as an Additive. *ACS Omega* **2020**, *5*, 27204–27210. [[CrossRef](#)] [[PubMed](#)]
2. Cüneyt Tas, A. Synthesis of biomimetic Ca-hydroxyapatite powders at 37 °C in synthetic body fluids. *Biomaterials* **2000**, *21*, 1429–1438. [[CrossRef](#)]
3. Gopi, D.; Shinyjoy, E.; Karthika, A.; Nithiya, S.; Kavitha, L.; Rajeswari, D.; Tang, T. Single walled carbon nanotubes reinforced mineralized hydroxyapatite composite coatings on titanium for improved biocompatible implant applications. *RSC Adv.* **2015**, *5*, 36766–36778. [[CrossRef](#)]
4. Šupová, M. Problem of hydroxyapatite dispersion in polymer matrices: A review. *J. Mater. Sci. Mater. Med.* **2009**, *20*, 1201–1213. [[CrossRef](#)] [[PubMed](#)]
5. Zhuang, Z.; Fujimi, T.J.; Nakamura, M.; Konishi, T.; Yoshimura, H.; Aizawa, M. Development of a,b-plane-oriented hydroxyapatite ceramics as models for living bones and their cell adhesion behavior. *Acta Biomater.* **2013**, *9*, 6732–6740. [[CrossRef](#)] [[PubMed](#)]
6. Melde, B.J.; Stein, A. Periodic Macroporous Hydroxyapatite-Containing Calcium Phosphates. *Chem. Mater.* **2002**, *14*, 3326–3331. [[CrossRef](#)]
7. Bernardi, G. Chromatography of Nucleic Acids on Hydroxyapatite. *Nature* **1965**, *206*, 779–783. [[CrossRef](#)]
8. Zhao, J.; Hu, Q.; Lei, Y.; Gao, C.; Zhang, P.; Zhou, B.; Zhang, G.; Song, W.; Lou, X.; Zhou, X. Facile synthesis of ultralong hydroxyapatite nanowires using wormlike micelles as soft templates. *CrystEngComm* **2021**, *23*, 5498–5503. [[CrossRef](#)]
9. Foroutan, R.; Peighambaroust, S.J.; Aghdasinia, H.; Mohammadi, R.; Ramavandi, B. Modification of bio-hydroxyapatite generated from waste poultry bone with MgO for purifying methyl violet-laden liquids. *Environ. Sci. Pollut. Res.* **2020**, *27*, 44218–44229. [[CrossRef](#)]
10. Ibrahim, M.; Labaki, M.; Giraudon, J.M.; Lamonier, J.F. Hydroxyapatite, a multifunctional material for air, water and soil pollution control: A review. *J. Hazard. Mater.* **2020**, *383*, 121139. [[CrossRef](#)]
11. Hao, L.; Lv, Y.; Song, H. The morphological evolution of hydroxyapatite on high-efficiency Pb²⁺ removal and antibacterial activity. *Microchem. J.* **2017**, *135*, 16–25. [[CrossRef](#)]
12. Sinusaite, L.; Popov, A.; Raudonyte-Svirbutaviciene, E.; Yang, J.-C.; Kareiva, A.; Zarkov, A. Effect of Mn doping on hydrolysis of low-temperature synthesized metastable alpha-tricalcium phosphate. *Ceram. Int.* **2021**, *47*, 12078–12083. [[CrossRef](#)]
13. Deng, Y.; Liu, M.; Chen, X.; Wang, M.; Li, X.; Xiao, Y.; Zhang, X. Enhanced osteoinductivity of porous biphasic calcium phosphate ceramic beads with high content of strontium-incorporated calcium-deficient hydroxyapatite. *J. Mater. Chem. B* **2018**, *6*, 6572–6584. [[CrossRef](#)] [[PubMed](#)]
14. Ravi, N.D.; Balu, R.; Sampath Kumar, T.S. Strontium-Substituted Calcium Deficient Hydroxyapatite Nanoparticles: Synthesis, Characterization, and Antibacterial Properties. *J. Am. Ceram. Soc.* **2012**, *95*, 2700–2708. [[CrossRef](#)]
15. Sekine, Y.; Motokawa, R.; Kozai, N.; Ohnuki, T.; Matsumura, D.; Tsuji, T.; Kawasaki, R.; Akiyoshi, K. Calcium-deficient Hydroxyapatite as a Potential Sorbent for Strontium. *Sci. Rep.* **2017**, *7*, 2064. [[CrossRef](#)]
16. Goto, T.; Kim, I.Y.; Kikuta, K.; Ohtsuki, C. Hydroxyapatite formation by solvothermal treatment of α -tricalcium phosphate with water–ethanol solution. *Ceram. Int.* **2012**, *38*, 1003–1010. [[CrossRef](#)]
17. Kaviyarasu, K.; Mariappan, A.; Neyvasagam, K.; Ayeshamariam, A.; Pandi, P.; Palanichamy, R.R.; Gopinathan, C.; Mola, G.T.; Maaza, M. Photocatalytic performance and antimicrobial activities of HAp-TiO₂ nanocomposite thin films by sol-gel method. *Surf. Interfaces* **2017**, *6*, 247–255. [[CrossRef](#)]

18. Teshima, K.; Lee, S.; Sakurai, M.; Kamenno, Y.; Yubuta, K.; Suzuki, T.; Shishido, T.; Endo, M.; Oishi, S. Well-Formed One-Dimensional Hydroxyapatite Crystals Grown by an Environmentally Friendly Flux Method. *Cryst. Growth Des.* **2009**, *9*, 2937–2940. [[CrossRef](#)]
19. Suchanek, K.; Bartkowiak, A.; Perzanowski, M.; Marszałek, M. From monetite plate to hydroxyapatite nanofibers by monoethanolamine assisted hydrothermal approach. *Sci. Rep.* **2018**, *8*, 15408. [[CrossRef](#)]
20. Tomozawa, M.; Hiromoto, S. Microstructure of hydroxyapatite- and octacalcium phosphate-coatings formed on magnesium by a hydrothermal treatment at various pH values. *Acta Mater.* **2011**, *59*, 355–363. [[CrossRef](#)]
21. Wang, Y.-c.; Wang, J.-n.; Xiao, G.-y.; Huang, S.-y.; Xu, W.-l.; Yan, W.-x.; Lu, Y.-p. Investigation of various fatty acid surfactants on the microstructure of flexible hydroxyapatite nanofibers. *CrystEngComm* **2021**, *23*, 7049–7055. [[CrossRef](#)]
22. Horiuchi, N.; Shibata, K.; Saito, H.; Iwabuchi, Y.; Wada, N.; Nozaki, K.; Hashimoto, K.; Tanaka, Y.; Nagai, A.; Yamashita, K. Size Control Synthesis of Hydroxyapatite Plates and Their Application in the Preparation of Highly Oriented Films. *Cryst. Growth Des.* **2018**, *18*, 5038–5044. [[CrossRef](#)]
23. Guo, X.; Xiao, P. Effects of solvents on properties of nanocrystalline hydroxyapatite produced from hydrothermal process. *J. Eur. Ceram. Soc.* **2006**, *26*, 3383–3391. [[CrossRef](#)]
24. Sinusaite, L.; Grigoraviciute-Puroniene, I.; Popov, A.; Ishikawa, K.; Kareiva, A.; Zarkov, A. Controllable synthesis of tricalcium phosphate (TCP) polymorphs by wet precipitation: Effect of washing procedure. *Ceram. Int.* **2019**, *45*, 12423–12428. [[CrossRef](#)]
25. Brunauer, S.; Emmett, P.H.; Teller, E. Adsorption of Gases in Multimolecular Layers. *J. Am. Chem. Soc.* **1938**, *60*, 309–319. [[CrossRef](#)]
26. Bogdanoviciene, I.; Beganskiene, A.; Tönsuaadu, K.; Glaser, J.; Meyer, H.J.; Kareiva, A. Calcium hydroxyapatite, $\text{Ca}_{10}(\text{PO}_4)_6(\text{OH})_2$ ceramics prepared by aqueous sol-gel processing. *Mater. Res. Bull.* **2006**, *41*, 1754–1762. [[CrossRef](#)]
27. Carrodeguas, R.G.; De Aza, S. α -Tricalcium phosphate: Synthesis, properties and biomedical applications. *Acta Biomater.* **2011**, *7*, 3536–3546. [[CrossRef](#)]
28. Sadat-Shojai, M.; Khorasani, M.-T.; Dinpanah-Khoshdargi, E.; Jamshidi, A. Synthesis methods for nanosized hydroxyapatite with diverse structures. *Acta Biomater.* **2013**, *9*, 7591–7621. [[CrossRef](#)]
29. Larsen, M.J.; Thorsen, A.; Jensen, S.J. Ethanol-induced formation of solid calcium phosphates. *Calcif. Tissue Int.* **1985**, *37*, 189–193. [[CrossRef](#)]
30. Lerner, E.; Azoury, R.; Sarig, S. Rapid precipitation of apatite from ethanol-water solution. *J. Cryst. Growth* **1989**, *97*, 725–730. [[CrossRef](#)]
31. Termine, J.D.; Peckauskas, R.A.; Posner, A.S. Calcium phosphate formation in vitro: II. Effects of environment on amorphous-crystalline transformation. *Arch. Biochem. Biophys.* **1970**, *140*, 318–325. [[CrossRef](#)]
32. Wu, J.; Lü, X.; Zhang, L.; Huang, F.; Xu, F. Dielectric Constant Controlled Solvothermal Synthesis of a TiO_2 Photocatalyst with Tunable Crystallinity: A Strategy for Solvent Selection. *Eur. J. Inorg. Chem.* **2009**, *2009*, 2789–2795. [[CrossRef](#)]
33. Wyman, J. The dielectric constant of mixtures of ethyl alcohol and water from -5 TO 40° . *J. Am. Chem. Soc.* **1931**, *53*, 3292–3301. [[CrossRef](#)]
34. Bohne, D.; Fischer, S.; Obermeier, E. Thermal, Conductivity, Density, Viscosity, and Prandtl-Numbers of Ethylene Glycol-Water Mixtures. *Ber. Der Bunsenges. Für Phys. Chem.* **1984**, *88*, 739–742. [[CrossRef](#)]
35. Ma, M.-G.; Zhu, Y.-J.; Chang, J. Monetite Formed in Mixed Solvents of Water and Ethylene Glycol and Its Transformation to Hydroxyapatite. *J. Phys. Chem. B* **2006**, *110*, 14226–14230. [[CrossRef](#)]
36. Thommes, M.; Kaneko, K.; Neimark, A.V.; Olivier, J.P.; Rodriguez-Reinoso, F.; Rouquerol, J.; Sing, K.S.W. Physisorption of gases, with special reference to the evaluation of surface area and pore size distribution (IUPAC Technical Report). *Pure Appl. Chem.* **2015**, *87*, 1051–1069. [[CrossRef](#)]